

Article

# Rheology of Pickering Emulsions Stabilized and Thickened by Cellulose Nanocrystals over Broad Ranges of Oil and Nanocrystal Concentrations

Saumay Kinra and Rajinder Pal \*

Department of Chemical Engineering, University of Waterloo, Waterloo, ON N2L 3G1, Canada; s2kinra@uwaterloo.ca

\* Correspondence: rpal@uwaterloo.ca

**Abstract:** The rheology of oil-in-water (O/W) emulsions, stabilized and thickened by cellulose nanocrystals, also referred to as nanocrystalline cellulose (NCC), was investigated over broad ranges of NCC and oil concentrations. The NCC concentration was varied from 1.03 to 7.41 wt% based on the aqueous phase. The oil concentration of the emulsion was varied from approximately 10 to 70 wt%. The emulsions produced were highly stable with respect to creaming and coalescence. The emulsions were non-Newtonian in that they exhibited strong shear-thinning behavior. The rheological data were described adequately by a power-law model. The consistency index ( $K$ ) and the flow behavior index ( $n$ ) of the emulsions were strongly dependent on the NCC and oil concentrations. At a fixed oil concentration, the consistency index increased whereas the flow behavior index decreased with the increase in NCC concentration. A similar behavior was observed when the NCC concentration was fixed and the oil concentration was increased; that is, the consistency index increased whereas the flow behavior index decreased.

**Keywords:** emulsion; nanocrystals; nanocrystalline cellulose; Pickering; rheology; viscosity; non-Newtonian; shear-thinning



**Citation:** Kinra, S.; Pal, R. Rheology of Pickering Emulsions Stabilized and Thickened by Cellulose Nanocrystals over Broad Ranges of Oil and Nanocrystal Concentrations. *Colloids Interfaces* **2023**, *7*, 36. <https://doi.org/10.3390/colloids7020036>

Academic Editors: Cecile Lemaitre and Philippe Marchal

Received: 17 March 2023

Revised: 9 April 2023

Accepted: 21 April 2023

Published: 24 April 2023



**Copyright:** © 2023 by the authors. Licensee MDPI, Basel, Switzerland. This article is an open access article distributed under the terms and conditions of the Creative Commons Attribution (CC BY) license (<https://creativecommons.org/licenses/by/4.0/>).

## 1. Introduction

Nanocrystalline cellulose (NCC), also referred to as cellulose nanocrystals (CNCs), is a promising low-cost nanomaterial for many novel applications [1–13]. It possesses unique properties such as: high stiffness (Young's modulus  $\approx 150$  GPa), high tensile strength ( $\approx 7500$  MPa), high aspect ratio ( $>15$ ), high surface area ( $>250$  m<sup>2</sup>/g), low density ( $\approx 1.5$  g/L), plenty of hydroxyl groups for functionalization, optical transparency, non-toxicity, biodegradability, and renewability.

NCC is produced from cellulose, the most abundant biopolymer on earth. Cellulose is a linear macromolecule of six-carbon rings (D-glucopyranose) linked with  $\beta$  (1–4) glycosidic bonds [9]. NCC is usually produced by sulfuric acid hydrolysis of amorphous portions of cellulose fibers. The cellulose macromolecules undergo two reactions simultaneously: the hydrolysis of glycosidic bonds and the esterification of surface hydroxyl groups. The hydrolysis of glycosidic bonds breaks the cellulose chains until the disordered regions are fully degraded and only the crystalline portions remain [10]. The esterification of surface hydroxyl groups forms anionic half-ester groups. The cellulose nanocrystals, when dispersed in water, carry a negative charge due to the presence of anionic half-ester groups.

The zeta potential of pristine cellulose nanocrystals extracted by sulfuric acid hydrolysis is typically in the range of  $-20$  to  $-50$  mV [4].

The applications of NCC are many. NCC can function as a barrier, lubricant, dispersant, thickener, and filler to improve the mechanical strength of polymer composites [14].

NCC greatly improves the gas barrier properties of packaging films when it is added to the polymeric matrix (poly lactic acid) of the packaging films. The permeability of the

film is greatly reduced due to the small particle size and high aspect ratio of cellulose nanocrystals [14]. NCC acts as a lubricant by reducing the coefficient of friction between surfaces and surface wear due to the alignment of the nanocrystals. NCC is also a good dispersant for the suspension of particles in liquids. The structure of cellulose nanocrystals allows stable suspension of particles. The high aspect ratio of NCC and the surface charge make cellulose nanocrystals excellent rheology modifiers. NCC thickens liquids and imparts shear-thinning properties to liquids [14].

Among the novel applications of NCC, the most important ones are fabrication of flexible and stretchable strain sensors [15–18], stretchable electroluminescent devices [19], flexible triboelectric nanogenerators [20], and recyclable/biodegradable packaging products [21]. As an example, consider the fabrication of flexible and stretchable strain sensors. The fabrication of such strain sensors requires a composite material consisting of extremely flexible elastomer such as polydimethylsiloxane (PDMS) filled with highly conductive filler such as carbon nanotubes or graphene (GN). The problem is that graphene is not easily dispersible in polymer matrix due to weak interactions between graphene and polymer. NCC is highly effective in dispersing GN in a polymer matrix. The NCC is first hydrophobically modified. The hydrophobically modified NCC (MNCC) forms nanocomplexes with GN. The MNCC-GN nanocomplexes are readily dispersible in elastomer due to the strong interaction between the nanocomplexes and the elastomer resulting in highly flexible and stretchable electrically conductive elastomer suitable for the fabrication of flexible and stretchable strain sensors.

The application of NCC in emulsion systems, where cellulose nanocrystals are employed for stabilization and thickening, is an area of great interest [22–30]. Emulsions are dispersions of two immiscible liquids such as oil and water that are stabilized by the presence of a surfactant or another stabilizer such as nanocrystals [22]. It is feasible to attain high levels of stability and control over the emulsion's properties, such as its viscosity and droplet size, by utilizing NCC as a stabilizer [22]. By interacting with the droplets and forming a physical barrier that stops them from coalescing, cellulose nanocrystals can be utilized to stabilize emulsions. Due to the abundance of hydroxyl groups present on the surface of nanocrystals, the nanocrystals are hydrophilic in nature. However, the presence of hydrophobic (200)  $\beta$  crystalline edges containing CH groups provides hydrophobicity to the nanocrystals [31,32]. The adsorption of nanocrystals at the surface of the oil droplets is facilitated by this hydrophobic–hydrophilic nature of nanocrystals. The hydrophobic edge of the nanocrystal aligns with the oil phase and the hydrophilic parts are exposed to the aqueous phase [33–36]. In addition to providing stability to emulsions, NCC can also be used as a rheology modifier to make the emulsion more viscous, which is beneficial for processes such as thickening food and cosmetic items [22].

Pickering emulsions stabilized with NCC have many potential applications in different fields such as food, pharmaceutical, cosmetics, catalysts, materials synthesis, and petroleum. As an example, Aw et al. [37] recently studied the use of cellulose nanocrystals to stabilize a Pickering oil-in-water emulsion the oil droplets of which were loaded with curcumin; a bioactive supplement commonly found in turmeric. The NCC-stabilized emulsion was found to be more stable and effective at preserving the curcumin than traditional stabilization methods.

The rheology of surfactant-stabilized emulsions has been studied extensively in literature [38–43] since the early twentieth century. However, the rheology of solids-stabilized Pickering emulsions has only received serious attention recently due to the availability of a variety of novel nanoparticles that can be used to stabilize the emulsions [44–57].

Miao et al. [55] investigated the rheology of Pickering oil-in-water emulsions stabilized by cellulose nanocrystals. The nanocrystal concentration varied from 0.6 to 2.4 wt%. However, this study was restricted to just two oil concentrations, that is 65 and 80 vol%. Velandia et al. [58] studied the viscosity and elasticity of Pickering water-in-oil emulsions stabilized by hydrophobic silica. The oil phase contained silica at 1 wt% concentration and the water concentration (volume fraction) varied from 0.1 to 0.75. Katepalli et al. [50]

studied the rheology of oil-in-water emulsion stabilized by fumed silica. The fumed silica was dispersed in the aqueous phase at a concentration of 2 wt%. The oil concentration was fixed at 50 vol%. In general, the published studies on the rheology of Pickering oil-in-water emulsions are restricted to a narrow range of oil and nanoparticle concentrations.

This article reports new results on the rheology of Pickering oil-in-water emulsions stabilized and thickened by cellulose nanocrystals. The unique aspect of this study is that it covers a broad range of nanocrystal and oil concentrations. The nanocrystal concentration varied from 1.03 to 7.41 wt% based on the matrix fluid (aqueous phase) and the oil concentration of the emulsion was varied from 0 to approximately 70 wt%. Thus, NCC was used both as a stabilizer of droplets and a rheology modifier of the matrix fluid.

## 2. Materials and Methods

Emulsions of the oil-in-water (O/W) type were prepared using deionized water containing 0.06 wt% NaCl, white mineral oil, and cellulose nanocrystals. The white mineral (Petro-Canada Purity FG WO-15) was supplied by Boucher and Jones Fuels, Waterloo (ON, Canada). The viscosity of the batch of oil used in this study was 27.62 mPa·s at 21 °C. The nanocrystalline cellulose (trade name: NCC NCV100-NASD90) was provided by CelluForce Inc., Windsor (ON, Canada). It was produced by sulfuric acid hydrolysis of wood pulp followed by spray-drying. It consisted of 3.4 sulfate half-ester groups per 100 D-glucopyranose rings, corresponding to sulfur to a carbon atomic ratio of about 0.0057 or 211 mmol/kg [3]. The cellulose nanocrystals were rod-shaped with a mean length of 76 nm and a mean width of 3.4 nm. The surface area of the cellulose nanocrystals was 500 m<sup>2</sup>/g and the crystallinity was 88% [3].

Figure 1 shows a schematic representation of the type of emulsions investigated in the present work. Note that cellulose nanocrystals are rod-shaped particles [3,59].

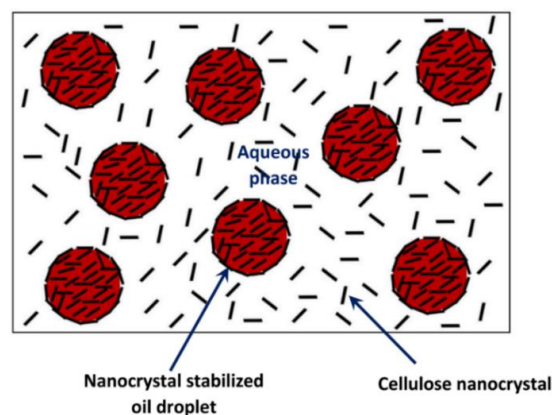


**Figure 1.** Schematic of the type of emulsions investigated in the present work.

The size distribution of cellulose nanocrystals was determined by DLS (dynamic light scattering) using a Zetasizer Nano ZS90 (Malvern Instruments Ltd., Worcester, UK) with a He-Ne laser operating at 633 nm frequency. The concentration of NCC solution used for particle size distribution measurement was 1 wt%. The size distribution of cellulose nanocrystals is shown in Figure 2. The mean hydrodynamic diameter of nanocrystals is approximately 24 nm.

### 2.1. Preparation of Nanocrystalline Cellulose Dispersions

The nanocrystalline cellulose dispersion was prepared at room temperature ( $22 \pm 1$  °C) by slowly adding a known amount of nanocrystals into a known amount of aqueous phase (deionized water containing 0.06 wt% NaCl) while maintaining mixing of the dispersion using a variable speed homogenizer (Gifford-Wood, model 1 L). It is of note that the addition of NaCl to the aqueous phase was carried out to screen the surface charge of NCC and, hence, to promote the interfacial packing of nanocrystals at the oil/water interface.

Bai et al. [57] also used 0.06 wt% NaCl in the preparation of NCC-stabilized oil-in-water emulsions. The dispersion was agitated in the homogenizer at high speed for at least 60 min until the nanocrystals were fully dispersed. The nanocrystal dispersion was left overnight to eliminate any air entrapped during the homogenization process. Eight dispersions of different nanocrystal concentrations ranging from 1.03 to 7.41 wt% were prepared. The nanocrystal concentration of the dispersion was increased in increments of approximately 1 wt%. The pH of NCC dispersions was approximately 8. Figure 3 shows the preparation process for dispersion of cellulose nanocrystals.

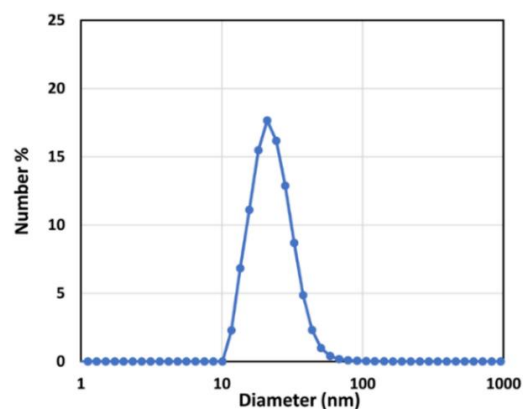


**Figure 2.** Size distribution of cellulose nanocrystals (1 wt% NCC solution).

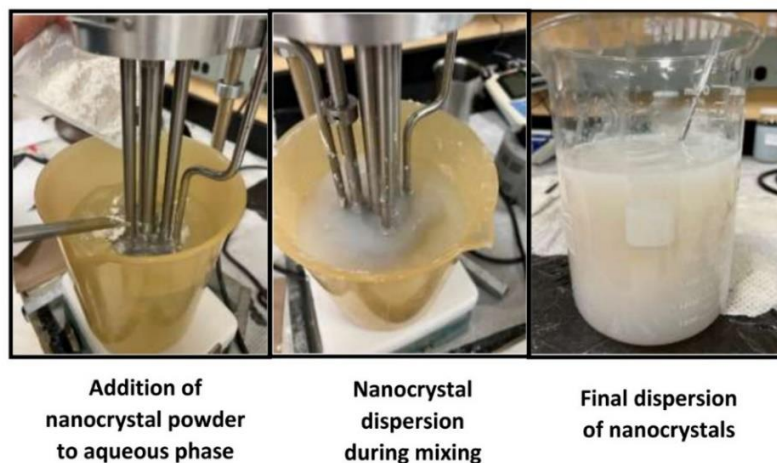


**Figure 3.** Preparation of dispersion of cellulose nanocrystals.

## 2.2. Preparation of O/W Emulsions

Emulsions of the oil-in-water (O/W) type were prepared at room temperature ( $22 \pm 1$  °C) by slowly adding a known amount of oil to a known amount of nanocellulose dispersion while maintaining mixing of the fluids using a homogenizer. After addition of the required amount of oil, the fluids were sheared in the homogenizer at high speed for at least 60 min. The emulsion which had been prepared in this way was left overnight to eliminate any air entrapped during the homogenization process. To prepare a higher oil concentration emulsion, a known amount of oil was added slowly to an existing lower concentration emulsion while maintaining mixing of the fluids in the homogenizer. After the addition of the oil, the fluids were sheared in the homogenizer at high speed for more than 60 min. The oil concentration of the emulsion was increased in increments of approximately 10 wt% until a concentration of 60 wt% was reached. At higher oil concentrations (>60 wt%), the oil concentration of the emulsion was increased in increments of approximately 5 wt%. The range of oil concentration for a given nanocellulose dispersion generally varied from 0 to approximately 70 wt%.

It should be noted that the emulsions prepared were O/W-type throughout. No phase inversion of O/W emulsion to W/O emulsion was observed. The type of emulsion was monitored using the electrical conductivity probe. O/W emulsions are electrically conductive, whereas W/O emulsions are non-conductive.

Table 1 gives complete information about the compositions of the emulsions investigated in this study. It should be noted that our goal was to scan the rheology of emulsions over the broad ranges of NCC and oil concentrations to fully capture the rheological behavior of emulsions. The NCC concentration varied in increments of about 1 wt% as this increment was sufficient to cause a significant change in the rheological properties. The oil concentration generally varied in increments of about 10 wt% as this increment in oil concentration was sufficient to cause a significant change in the rheological properties of the emulsion.

**Table 1.** Compositions of emulsions investigated in this study.

Nanocrystal Concentration of Matrix Phase (wt%)	Oil Concentration of Emulsion (wt%)	Oil Concentration of Emulsion (vol%)
1.03	Seven concentrations: 10.49, 28.42, 40.38, 50.32, 60.28, 65.27, 70.26	Seven concentrations: 12.17, 31.93, 44.45, 54.47, 64.20, 68.95, 73.62
1.99	Eight concentrations: 10.10, 20.16, 30.15, 40.13, 50.12, 60.10, 65.10, 70.12	Eight concentrations: 11.75, 23.03, 33.84, 44.27, 54.35, 64.10, 68.85, 73.55
2.91	Eight concentrations: 10.01, 20.01, 30.03, 40.05, 50.06, 60.05, 65.07, 70.09	Eight concentrations: 11.68, 22.92, 33.79, 44.26, 54.37, 64.12, 68.89, 73.59
3.85	Eight concentrations: 10.03, 20.04, 30.06, 40.05, 50.06, 60.06, 65.07, 70.07	Eight concentrations: 11.73, 23.01, 33.89, 44.34, 54.45, 64.20, 68.96, 73.73
4.77	Eight concentrations: 10.05, 20.04, 30.04, 40.05, 50.06, 60.07, 65.07, 70.07	Eight concentrations: 11.79, 23.07, 33.94, 44.42, 54.53, 64.28, 69.03, 73.69
5.66	Eight concentrations: 10.02, 20.03, 30.04, 40.07, 50.09, 60.08, 65.08, 70.08	Eight concentrations: 11.78, 23.11, 34.01, 44.52, 54.64, 64.36, 69.10, 73.75
6.55	Eight concentrations: 10.01, 20.04, 30.04, 40.05, 50.06, 60.08, 65.08, 70.08	Eight concentrations: 11.81, 23.17, 34.07, 44.58, 54.68, 64.43, 69.16, 73.81
7.41	Seven concentrations: 10.03, 20.06, 30.05, 40.07, 50.06, 60.07, 65.07	Seven concentrations: 11.86, 23.25, 34.15, 44.67, 54.76, 64.49, 69.22

### 2.3. Measurements

Two co-axial cylinder viscometers, namely Fann and Haake viscometers, were used to carry out the rheological measurements. The relevant dimensions of the devices are given in Table 2. In the Fann viscometer, the inner cylinder is kept stationary, whereas the outer cylinder rotates. There are 12 speeds ranging from 0.9 to 600 rpm. In the Haake viscometer, the inner cylinder rotates, and the outer cylinder is held stationary. There are 30 speeds ranging from 0.01 to 512 rpm. The viscometers were calibrated using the standards of known viscosities. The viscosity measurements were carried out at room temperature ( $22 \pm 1$  °C).

**Table 2.** Relevant dimensions of viscometers used in this study.

Device	Inner Cylinder Radius, $R_i$ (cm)	Outer Cylinder Radius, $R_o$ (cm)	Length of Inner Cylinder (cm)	Gap-Width (cm)
Fann 35A/SR-12	1.72	1.84	3.8	0.12
Haake Roto- visco RV 12 with MV I	2.00	2.1	6.0	0.10
Haake Roto- visco RV 12 with MV III	1.52	2.1	6.0	0.58

The droplets of emulsions were observed using a Zeiss optical microscope with transmitted light. The photomicrographs of emulsion droplets were taken using a camera. The emulsion samples were diluted with the aqueous phase before observation under the microscope.

### 3. Results and Discussion

#### 3.1. Rheology of Nanocrystalline Cellulose Dispersions

Figure 4 shows the physical appearance of nanocrystalline cellulose dispersions at concentrations ranging from 1.03 to 7.41 wt%. The dispersions are cloudy in appearance indicating aggregation of nanocrystals.

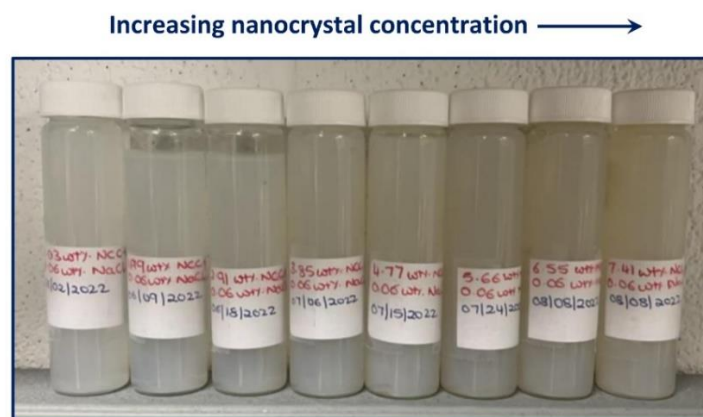


**Figure 4.** Physical appearance of NCC dispersions in order of increasing NCC concentration from 1.03 to 7.41 wt%.

The viscous flow behavior of the dispersions of cellulose nanocrystals is shown in Figure 5. The nanocrystal dispersion is only Newtonian at a low NCC concentration of 1.03 wt%; the viscosity is constant independent of the shear rate. The NCC dispersions become non-Newtonian shear-thinning at higher NCC concentrations. The viscosity decreases with the increase in shear rate for a given NCC dispersion. Additionally, the viscosity of nanocrystal dispersion increases with the increase in NCC concentration at a fixed shear rate. Interestingly, the viscous behavior of all non-Newtonian nanocrystalline cellulose dispersions can be described adequately using the power-law model:

$$\tau = K\dot{\gamma}^n \quad (1)$$

$$\eta = \tau/\dot{\gamma} = K\dot{\gamma}^{n-1} \quad (2)$$

where  $\tau$  is the shear stress,  $\dot{\gamma}$  is the shear rate,  $K$  is the consistency index,  $n$  is the flow-behavior index, and  $\eta$  is the viscosity. According to the power law model, Equation (2), the plot of viscosity versus shear rate on a log–log scale is expected to be linear as observed in Figure 5. From the slope and intercept of the line, the flow behavior index ( $n$ ) and consistency index ( $K$ ) are determined.

The flow behavior index  $n$  decreases sharply with the increase in nanocrystal concentration, indicating that the NCC dispersions become more shear-thinning as the nanocrystal concentration is increased. At high NCC concentrations larger than 6 wt%, the flow behavior index levels off. However, the consistency index  $K$  increases sharply with the increase in NCC concentration, especially when NCC concentration is above 4 wt%. Thus, dispersions of nanocrystalline cellulose become more shear-thinning and viscous with the increase in NCC concentration. The sharp increase in the consistency index  $K$  above 4 wt% NCC is likely due to the formation of liquid crystals. Previous studies [59] on NCC dispersions indicate that the dispersions are isotropic up to about 3 wt%. At higher NCC concentrations, the dispersion phase separates into crystalline and isotropic domains [59–62]. The shear-thinning behavior of NCC dispersions is due to the orientation of crystalline domains and individual rod-shaped nanocrystals in the direction of shear.

Figure 6 shows the STEM (Scanning Transmission Electron Microscopy) micrograph of an NCC sample consisting of 1 wt% NCC solution. The STEM was carried out with a Libra 200 MC manufactured by Carl Zeiss using the drop-cast method. The image was obtained

with a 200 keV monochromatized electron beam and a High-Angle Annular Dark-Field (HAADF) detector. The white regions of the image show the network of aggregates of rod-shaped nanocrystals. Figure 7 shows the AFM (atomic force microscopy) image of cellulose nanocrystals [14]. The image was supplied by the manufacturer of NCC, that is, CelluForce Inc. [14]. The AFM image is consistent with the STEM image clearly showing the network of aggregates of rod-shaped nanocrystals.

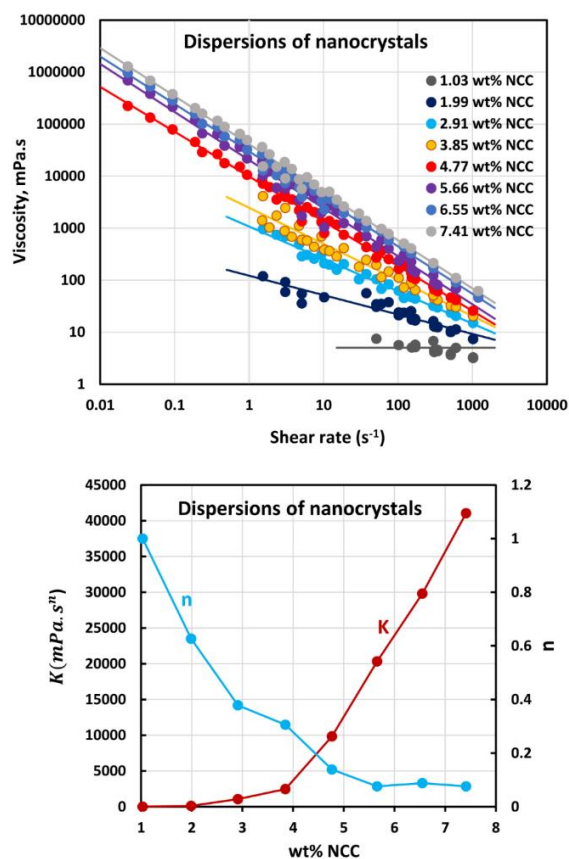


Figure 5. Viscous flow behavior of dispersions of cellulose nanocrystals.

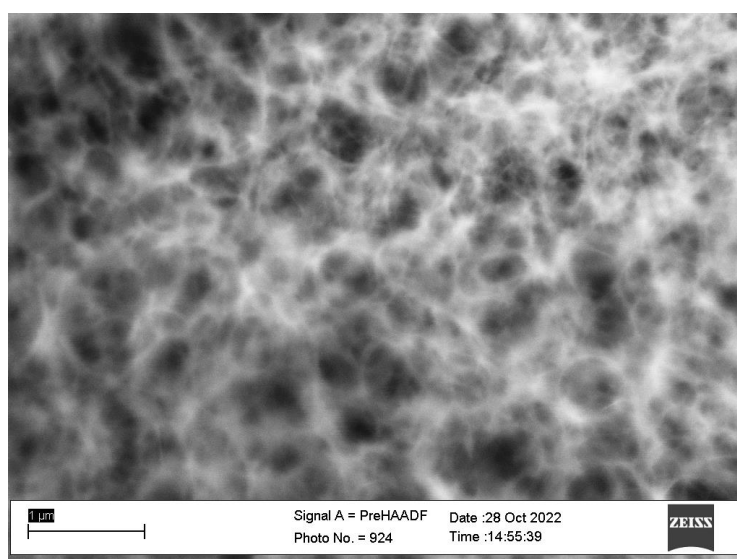
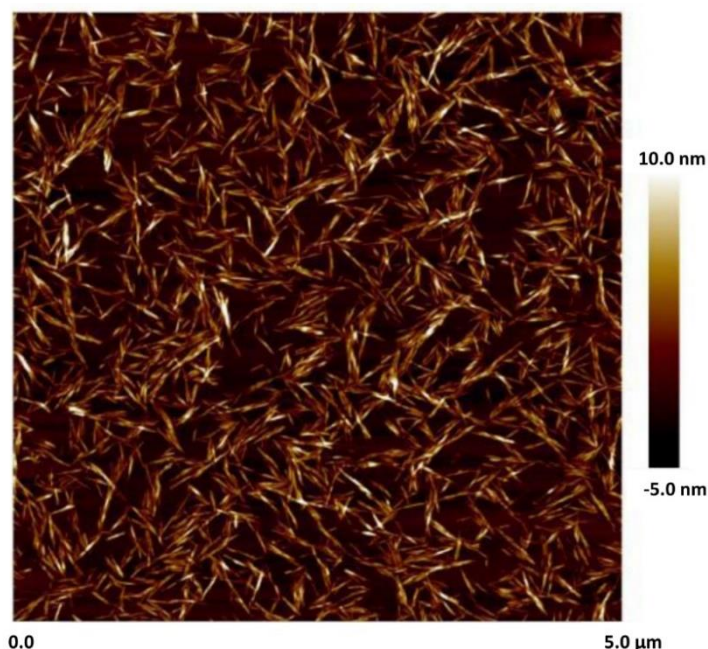


Figure 6. STEM (Scanning Transmission Electron Microscopy) image of dried sample of 1 wt% NCC solution.



**Figure 7.** Atomic force microscopy (AFM) image of cellulose nanocrystals [14].

### 3.2. Rheology of O/W Emulsions Stabilized and Thickened by Nanocrystalline Cellulose

Figures 8–11 show the viscous flow behaviors of O/W emulsions stabilized and thickened by cellulose nanocrystals. In each figure (parts (a) and (b)), the NCC concentration is fixed, but the oil concentration is varied. The figures reveal the following important characteristics of O/W emulsions stabilized and thickened by cellulose nanocrystals:

- Emulsions are Newtonian at low oil concentrations ( $\phi \leq 0.32$ ) and low NCC concentration ( $\leq 1.03$  wt%).
- Emulsions are shear-thinning non-Newtonian; that is, viscosity decreases with the increase in shear rate, when the NCC concentration is  $\geq 1.99$  wt%, regardless of the oil concentration.
- The viscous flow behavior of emulsions can be described very well using the power law model (see Equations (1) and (2)); that is, the decrease in viscosity with the increase in shear rate exhibits a linear relationship on a log–log plot.
- The consistency index  $K$  increases with the increase in oil concentration at any given NCC concentration.
- The flow behavior index  $n$  of non-Newtonian emulsions is generally well below a value of unity indicating a severe shear-thinning nature of emulsions.

Figure 12 compares the consistency index  $K$  and flow behavior index  $n$  values for O/W emulsions stabilized and thickened with different concentrations of nanocrystalline cellulose. For any given nanocrystal concentration, the consistency index increases with the increase in oil concentration. However, the increase in  $K$  with the increase in oil concentration is more severe at low NCC concentrations. At high NCC concentrations, the increase in  $K$  with the increase in oil concentration is only modest. The consistency index also increases with the increase in NCC concentration at a fixed oil concentration. For a given NCC concentration, the flow behavior index  $n$  is nearly constant with the increase in oil concentration up to a certain oil concentration. However, the index value drops sharply to lower values at high oil concentrations. For a fixed oil concentration, the flow behavior index drops substantially with the increase in NCC concentration.

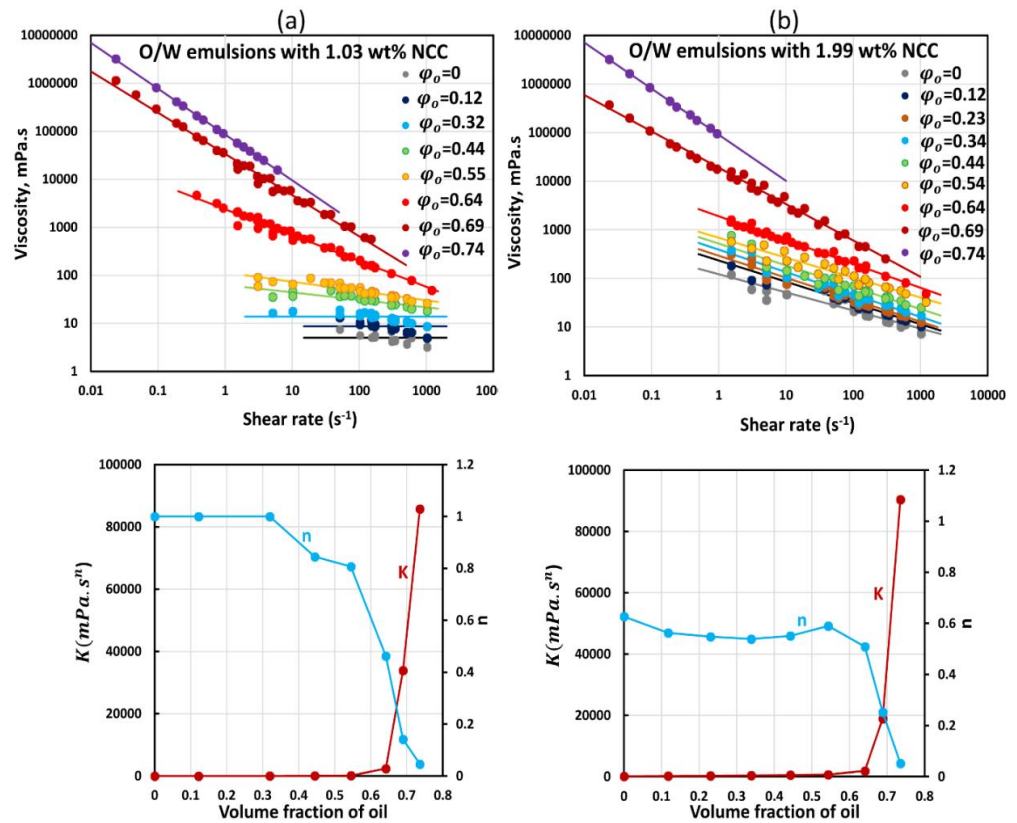


**Figure 8.** Viscous flow behavior of O/W emulsions at different volume fractions of oil ( $\varphi_o$ ) at a fixed NCC concentration: (a) NCC concentration of 1.03 wt%, and (b) NCC concentration of 1.99 wt%.

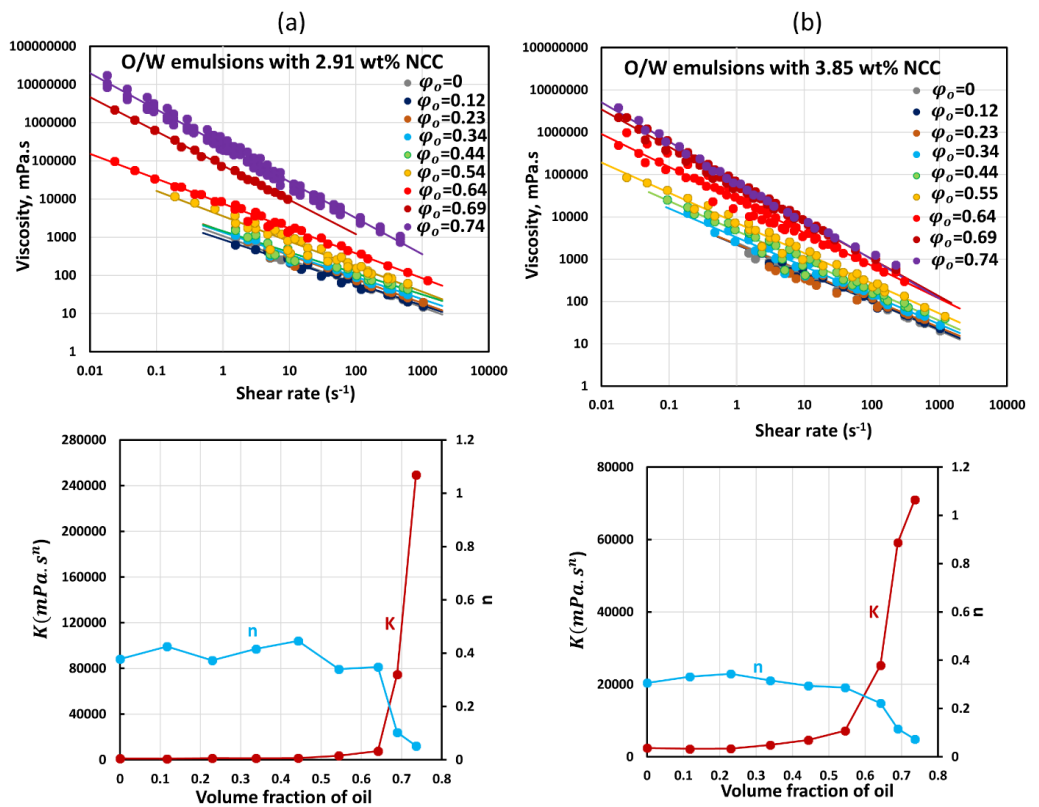


**Figure 9.** Viscous flow behavior of O/W emulsions at different volume fractions of oil ( $\varphi_o$ ) at a fixed NCC concentration: (a) NCC concentration of 2.91 wt%, and (b) NCC concentration of 3.85 wt%.

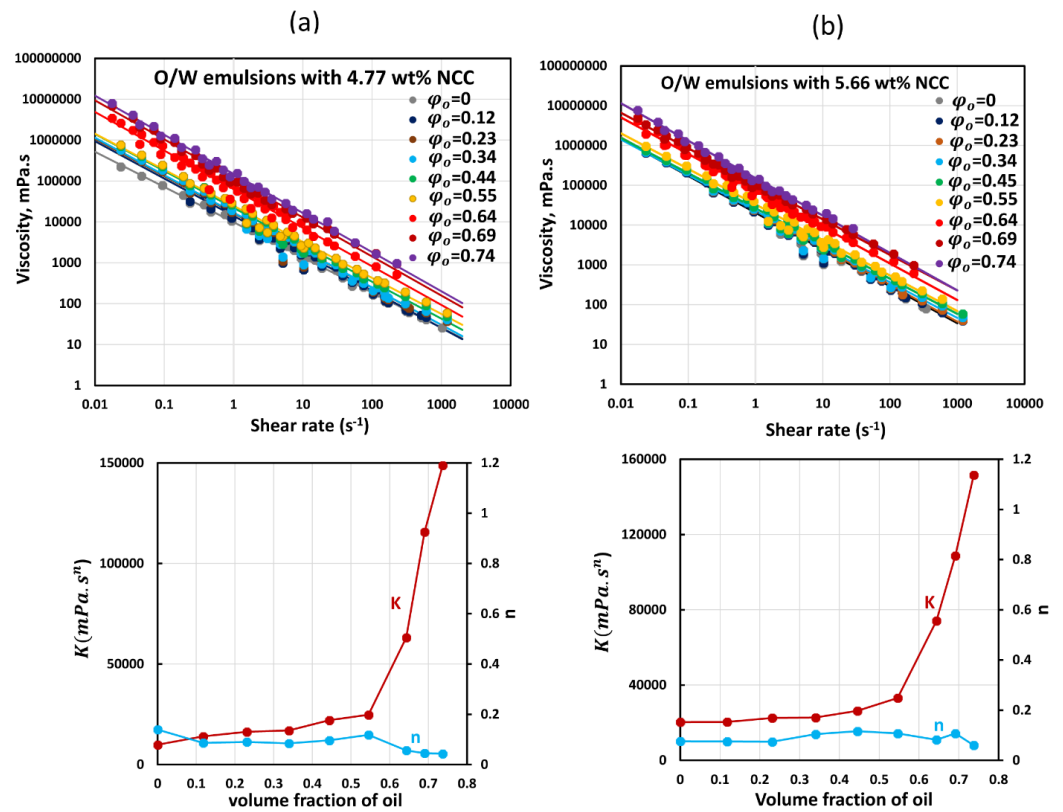


**Figure 10.** Viscous flow behavior of O/W emulsions at different volume fractions of oil ( $\varphi_o$ ) at a fixed NCC concentration: (a) NCC concentration of 4.77 wt%, and (b) NCC concentration of 5.66 wt%.

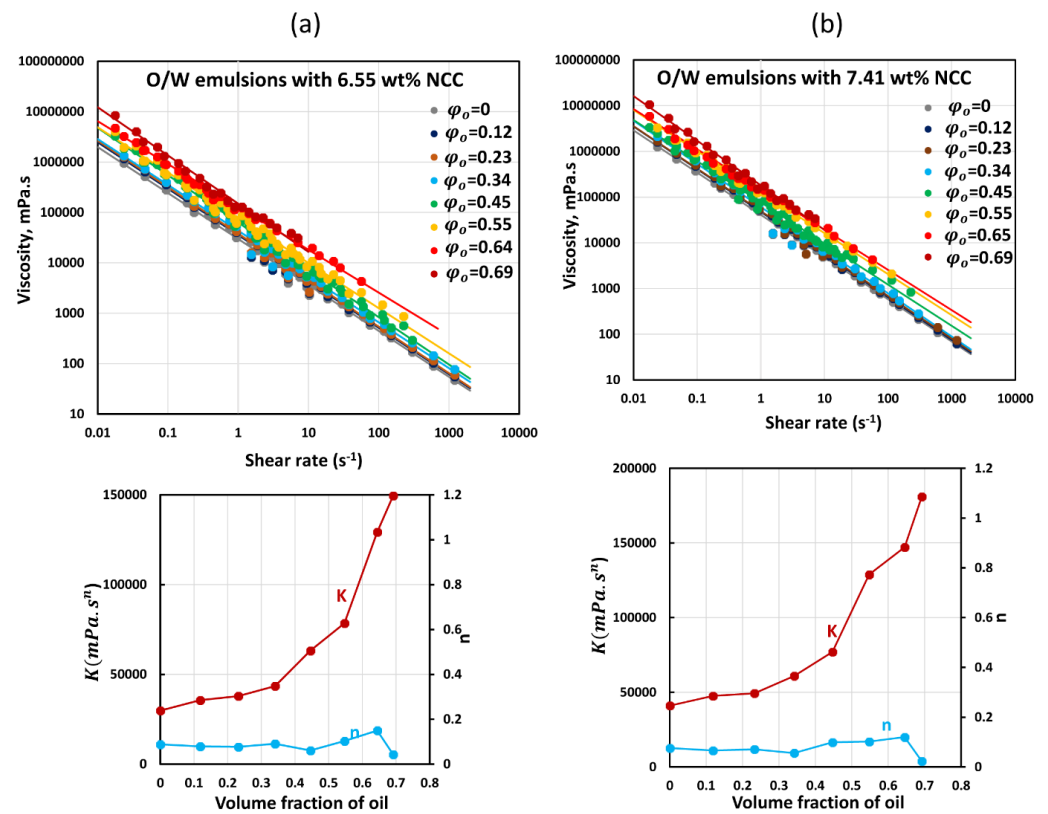


**Figure 11.** Viscous flow behavior of O/W emulsions at different volume fractions of oil ( $\varphi_o$ ) at a fixed NCC concentration: (a) NCC concentration of 6.55 wt%, and (b) NCC concentration of 7.41 wt%.

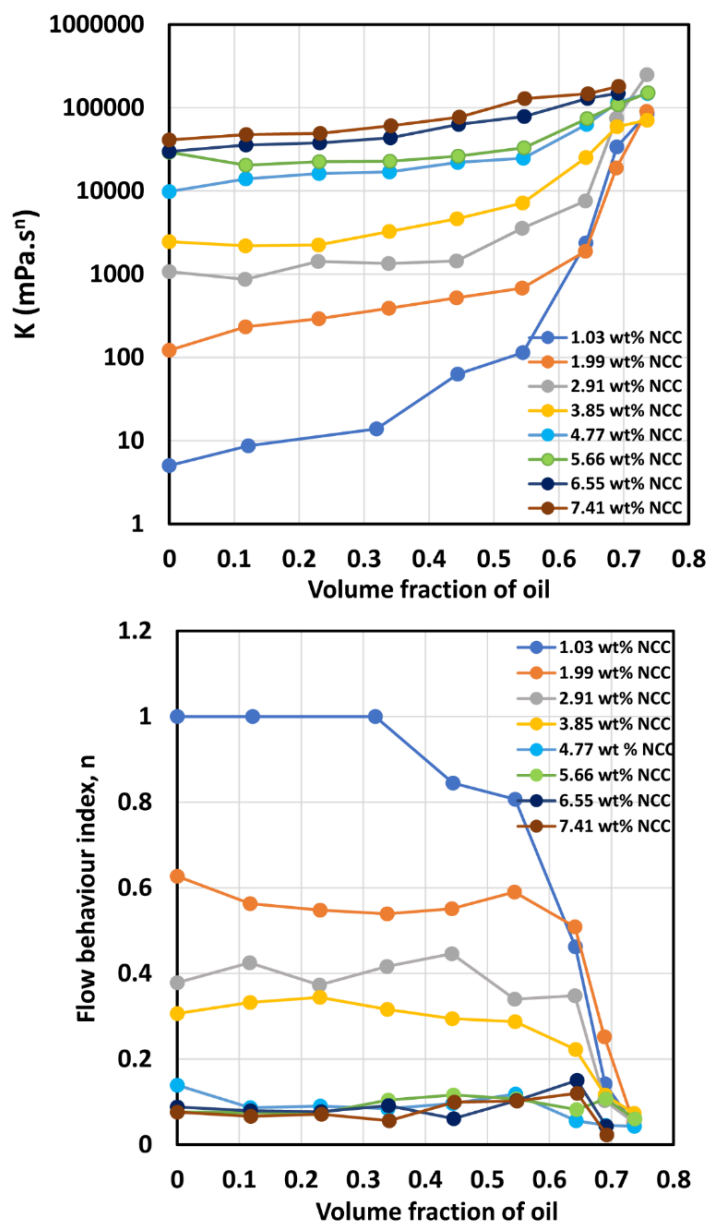


**Figure 12.** Comparison of consistency index ( $K$ ) and flow behavior index ( $n$ ) of O/W emulsions thickened and stabilized with different concentrations of nanocrystalline cellulose (NCC).

When the NCC concentration of emulsion for a fixed oil concentration, is increased the viscosity of the matrix fluid is increased. As the viscosity of emulsion is directly proportional to the viscosity of matrix fluid [38,40], the viscosity, and hence the consistency index  $K$  of emulsion, increases accordingly. Increasing the NCC concentration of emulsion for a fixed oil concentration also makes the matrix fluid more shear-thinning. Consequently, the emulsion becomes more shear-thinning with a corresponding drop in the flow behavior index  $n$ .

When the oil concentration of emulsion for a fixed NCC concentration is increased, the viscosity, and hence consistency index  $K$  of emulsion, increases as oil droplets act as obstacles to flow resulting in an increase of flow resistance. The enhancement of shear-thinning, and hence a decrease in flow behavior index  $n$  of emulsion, with the increase in oil concentration is due to the following mechanisms: (a) break-up of aggregates of droplets occurs with the increase in shear rate, (b) deformation and orientation of droplets occurs with the increase in shear rate [38]. With the increase in shear rate, the aggregates of droplets undergo break-up, thereby releasing the entrapped matrix fluid and, hence, resulting in

lower emulsion viscosity. With the increase in shear rate, the droplets also become more elongated and oriented in the direction of flow, resulting in lower emulsion viscosity.

### 3.3. Physical Appearance and Stability of Emulsions

Figures 13 and 14 show samples of O/W emulsions stabilized and thickened by nanocrystalline cellulose at 50 and 70 wt% oil concentrations. At 50 wt% oil concentration (Figure 13), the emulsion has the consistency of a mobile fluid at low NCC concentrations. The emulsions have a paste-like consistency at high NCC concentrations. However, at a higher oil concentration of 70 wt% (Figure 14), the emulsions have a paste-like consistency at all NCC concentrations.

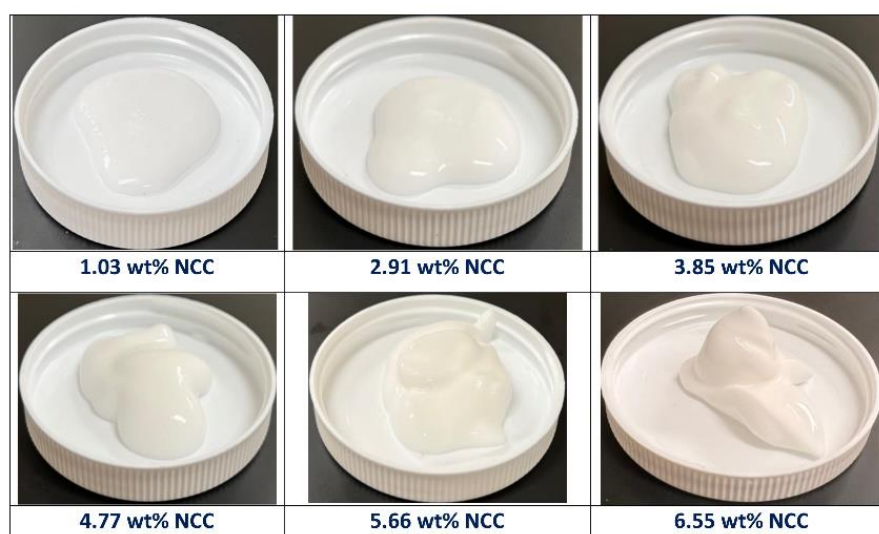


**Figure 13.** O/W emulsion samples with different concentrations of cellulose nanocrystals at a fixed oil concentration of 50 wt%.

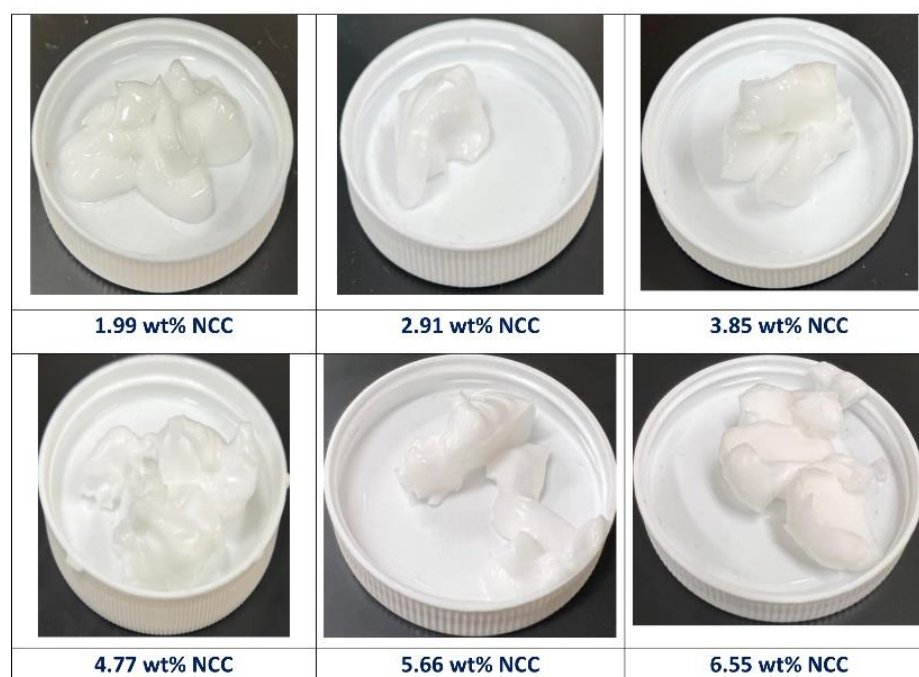


**Figure 14.** O/W emulsion samples with different concentrations of cellulose nanocrystals at a fixed oil concentration of 70 wt%.

The emulsions produced were highly stable with respect to creaming and coalescence at all concentrations of NCC and oil investigated. The emulsion samples stored for more than two months exhibited no creaming and coalescence of emulsion droplets. As can be seen in Figures 15 and 16, there is no separate aqueous phase layer formed at the bottom of the bottles to indicate the creaming of droplets. Additionally, there is no oil layer formed at the top of the bottles to indicate the coalescence of droplets.

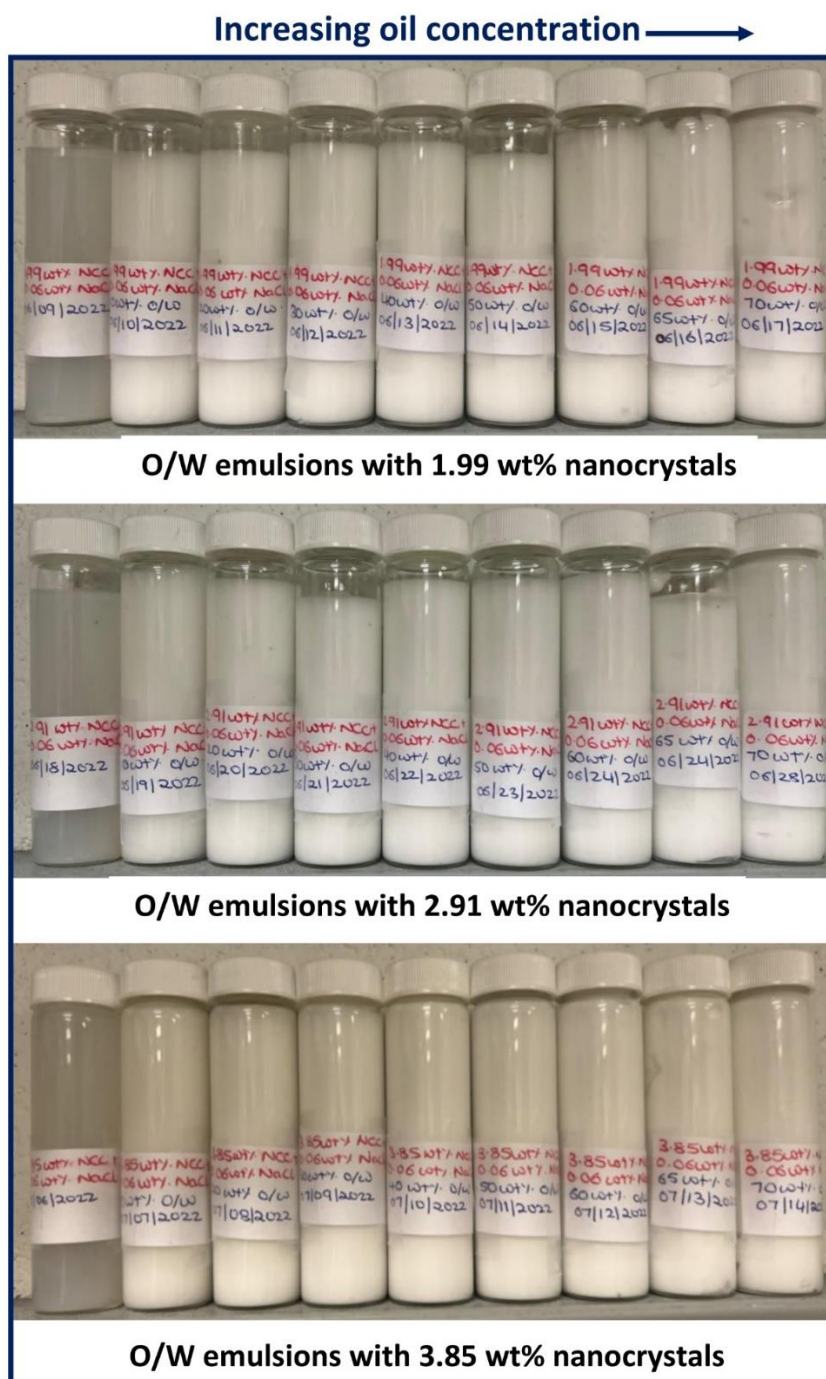


**Figure 15.** Samples of O/W emulsions when left unstirred for more than two months (NCC concentration range of 1.99 to 3.85 wt%; oil concentration range of 0 to 70 wt%).

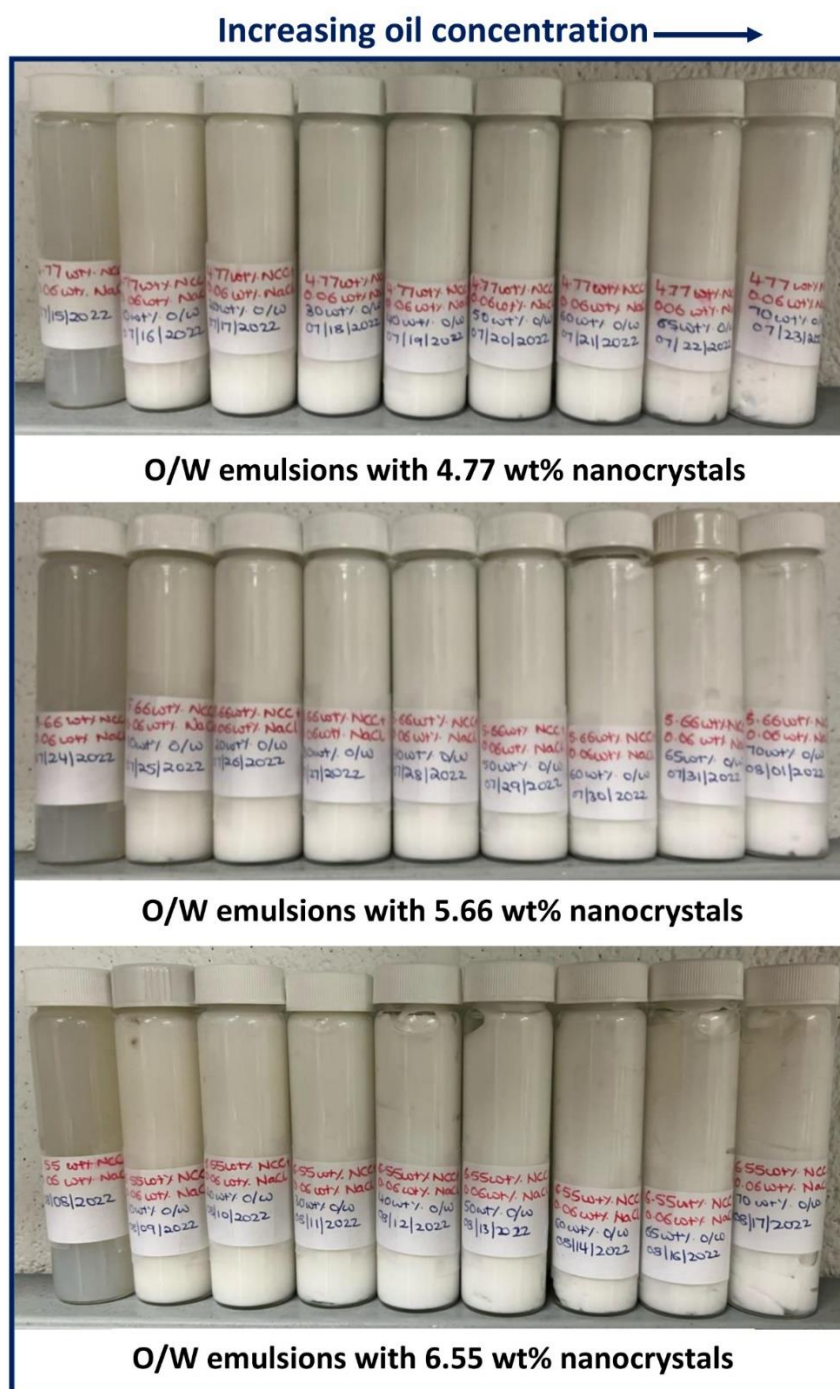


**Figure 16.** Samples of O/W emulsions when left unstirred for more than two months (NCC concentration range of 4.77 to 6.55 wt%; oil concentration range of 0 to 70 wt%).

### 3.4. Droplet Size of Emulsions

Figure 17 shows the typical photomicrograph of an emulsion sample. The photomicrographs were used to determine the droplet sizes of emulsions at different NCC and oil concentrations. The Sauter mean diameter of the emulsions ranged from 20  $\mu\text{m}$  to 100  $\mu\text{m}$  depending upon the NCC and oil concentrations. The Sauter mean diameter generally increased with the increase in oil concentration. This can be seen in Figure 18 which shows the variation of Sauter mean diameter with oil concentration at a fixed NCC concentration of 5.66 wt%. With the increase in NCC concentration at a fixed oil concentration, the Sauter

mean diameter generally decreased. This can be seen clearly in Figure 19 at a fixed oil concentration of 40 wt%.

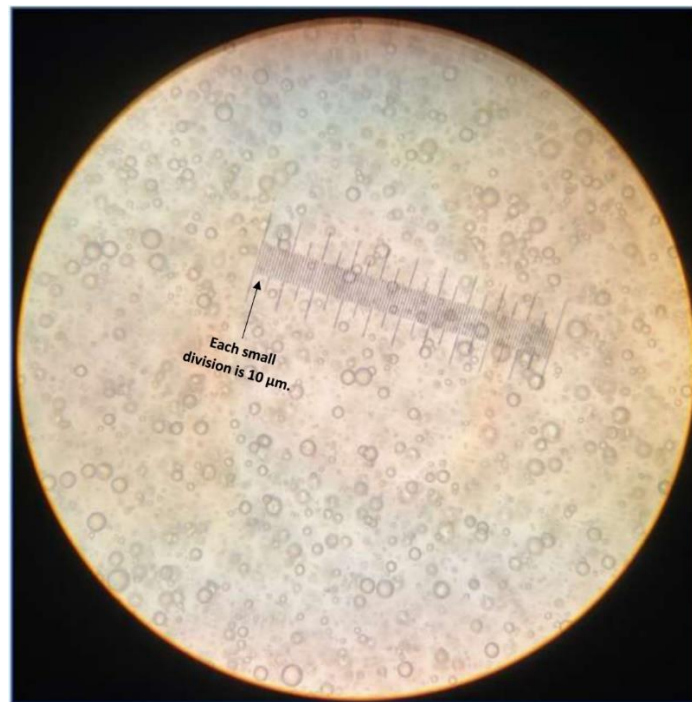


Figure 17. Typical photomicrograph of O/W emulsion stabilized and thickened by nanocrystalline cellulose.

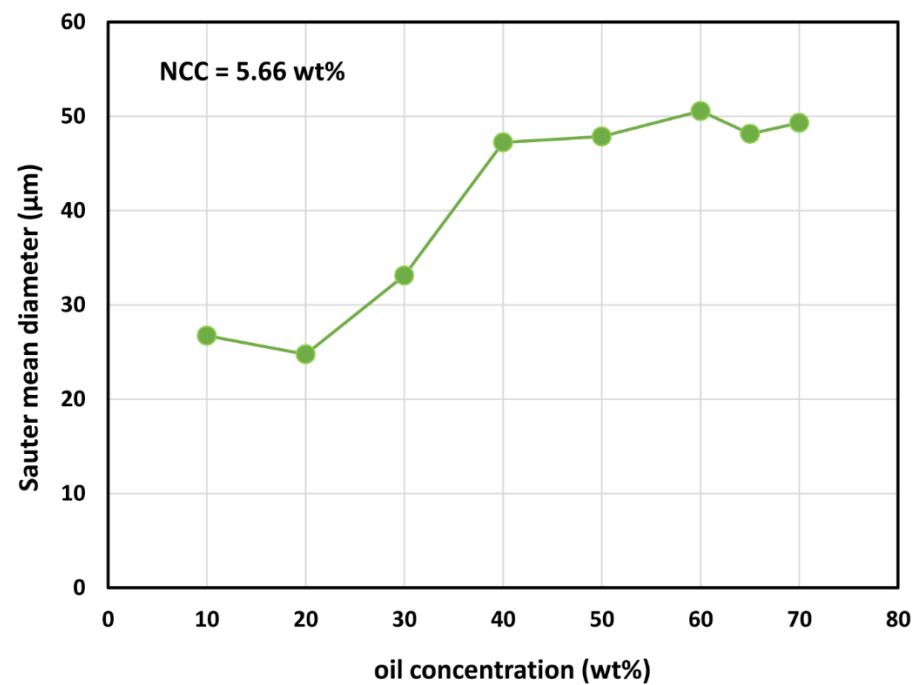
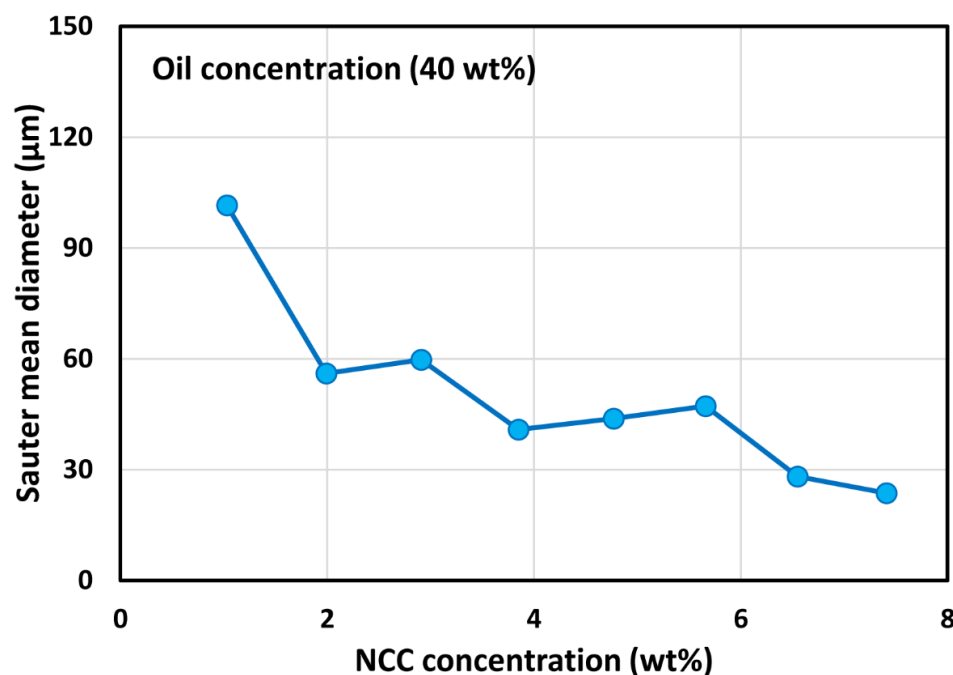


Figure 18. Effect of oil concentration on Sauter mean diameter at NCC concentration of 5.66 wt%.



**Figure 19.** Effect of NCC concentration on Sauter mean diameter at oil concentration of 40 wt%.

Previous studies on the rheology of emulsions [40] have shown that the viscosity of emulsions is inversely related to the mean droplet size; that is, the viscosity increases with the decrease in mean droplet size. In the present study, it is not possible to delineate the effect of mean droplet size on the viscosity of emulsions as other variables affecting the viscosity of emulsions are not held constant. For example, the droplet size changes are observed with the variations of NCC and oil concentrations, but the NCC and oil concentrations also have a direct effect on the viscosity of emulsions regardless of the droplet size.

#### 4. Conclusions

Based on the experimental work and data analysis, the following conclusions can be made: (1) Dispersions of nanocrystalline cellulose (NCC) are non-Newtonian shear-thinning at NCC concentrations larger than 1.03 wt%. The rheological behavior of non-Newtonian NCC dispersions can be described adequately by a power-law model. The consistency index increases whereas the flow behavior index decreases with the increase in NCC concentration; (2) The O/W emulsions stabilized and thickened by cellulose nanocrystals are Newtonian only at low concentrations of NCC ( $\leq 1.03$  wt%) and low volume fractions of oil ( $\varphi_o \leq 0.32$ ). In general, the emulsions are non-Newtonian shear-thinning in nature; (3) The rheological behavior of non-Newtonian O/W emulsions can be described adequately by a power-law model. The consistency index increases with the increases in NCC and oil concentrations whereas the flow behavior index decreases with the increases in NCC and oil concentrations; (4) The O/W emulsions produced were highly stable with respect to creaming and coalescence indicating that cellulose nanocrystals are highly effective stabilizers for O/W emulsions; (5) The average droplet size of O/W emulsions stabilized and thickened by nanocrystalline cellulose generally decreased with the increase in NCC concentration and increased with the increase in oil concentration.

**Author Contributions:** Conceptualization, R.P.; methodology, S.K. and R.P.; validation, S.K. and R.P.; formal analysis, R.P.; investigation, S.K. and R.P.; resources, R.P.; data curation, S.K.; writing—original draft preparation, R.P.; writing—review and editing, R.P.; visualization, R.P.; supervision, R.P.; project administration, R.P.; funding acquisition, R.P. All authors have read and agreed to the published version of the manuscript.

**Funding:** This research was funded by the Discovery Grant awarded to R.P. by the Natural Sciences and Engineering Research Council of Canada.

**Data Availability Statement:** The data presented in this study are available on request from corresponding author.

**Conflicts of Interest:** The authors declare no conflict of interest.

## References

1. Prathapan, R.; Thapa, R.; Garnier, G.; Tabor, R.F. Modulating the zeta potential of cellulose nanocrystals using salts and surfactants. *Colloids Surf. A Physicochem. Eng. Asp.* **2016**, *509*, 11–18. [[CrossRef](#)]
2. Lu, P.; Hsieh, Y. Preparation and properties of cellulose nanocrystals: Rods, spheres, and network. *Carbohydr. Polym.* **2010**, *82*, 329–336. [[CrossRef](#)]
3. Girard, M.; Vidal, D.; Bertrand, F.; Tavares, J.R.; Heuzey, M. Evidence-based guidelines for the ultrasonic dispersion of cellulose nanocrystals. *Ultrason. Sonochem.* **2021**, *71*, 105378. [[CrossRef](#)] [[PubMed](#)]
4. Shojaeiarani, J.; Bajwa, D.S.; Chanda, S. Cellulose nanocrystal-based composites: A review. *Compos. Part C Open Access* **2021**, *5*, 100164. [[CrossRef](#)]
5. Yang, X.; Biswas, S.K.; Han, J.; Tanpichai, S.; Li, M.; Chen, C.; Zhu, S.; Das, A.K.; Yano, H. Surface and interface engineering for nanocellulosic advanced materials. *Adv. Mater.* **2021**, *33*, 2002264. [[CrossRef](#)] [[PubMed](#)]
6. Trache, D.; Hussin, M.H.; Haafiz, M.K.M.; Thakur, V.K. Recent progress in cellulose nanocrystals: Sources and production. *Nanoscale* **2017**, *9*, 1763–1786. [[CrossRef](#)]
7. Aziz, T.; Fan, H.; Zhang, X.; Haq, A.; Ullah, R.; Khan, F.U.; Iqbal, M. Advance study of cellulose nanocrystals properties and applications. *J. Polym. Environ.* **2020**, *28*, 1117–1128. [[CrossRef](#)]
8. Aziz, T.; Ullah, A.; Fan, H.; Ullah, R.; Haq, F.; Khan, F.U.; Iqbal, M.; Wei, J. Cellulose nanocrystals applications in health, medicine, and catalysis. *J. Polym. Environ.* **2021**, *29*, 2062–2071. [[CrossRef](#)]
9. Dufresne, A. Nanocellulose processing properties and potential applications. *Curr. For. Rep.* **2019**, *5*, 76–89. [[CrossRef](#)]
10. Vanderfleeth, O.M.; Cranston, E.D. Production routes to tailor the performance of cellulose nanocrystals. *Nat. Rev. Mater.* **2021**, *6*, 124–144. [[CrossRef](#)]
11. Panchal, P.; Ogunsona, E.; Mekonnen, T. Trends in advanced functional material applications of nanocellulose. *Processes* **2019**, *7*, 10. [[CrossRef](#)]
12. Zhang, H.; Dou, C.; Pal, L.; Hubbe, M.A. Review of electrically conductive composites and films containing cellulosic fibers or nanocellulose. *BioResources* **2019**, *14*, 7494–7542. [[CrossRef](#)]
13. Gupta, A.; Mekonnen, T.H. Cellulose nanocrystals enabled sustainable polycaprolactone based shape memory polyurethane bionanocomposites. *J. Colloid Interface Sci.* **2022**, *611*, 726–738. [[CrossRef](#)]
14. Cellulose Nanocrystals (CNC). Available online: <https://cellulforce.com/cellulose-nanocrystals-cnc/> (accessed on 26 February 2023).
15. Zhu, S.; Lu, Y.; Wang, S.; Sun, H.; Yue, Y.; Xu, X.; Mei, C.; Xiao, H.; Fu, Q.; Han, J. Interface design of stretchable and environment-tolerant strain sensors with hierarchical nanocellulose-supported graphene nanocomplexes. *Compos. Part A Appl. Sci. Manuf.* **2023**, *164*, 107313. [[CrossRef](#)]
16. Lu, Y.; Yue, Y.; Ding, Q.; Mei, C.; Xu, X.; Wu, Q.; Xiao, H.; Han, J. Self-recovery, fatigue-resistant, and multifunctional sensor assembled by a nanocellulose/carbon nanotube nanocomplex-mediated hydrogel. *Appl. Mater. Interfaces* **2021**, *13*, 50281–50297. [[CrossRef](#)]
17. Zhu, S.; Sun, H.; Lu, Y.; Wang, S.; Yue, Y.; Xu, X.; Mei, C.; Xiao, H.; Fu, Q.; Han, J. Inherently conductive poly(dimethylsiloxane) elastomers synergistically mediated by nanocellulose/carbon nanotube nanohybrids toward highly sensitive, stretchable, and durable strain sensors. *Appl. Mater. Interfaces* **2021**, *13*, 59142–59153. [[CrossRef](#)]
18. Zhou, J.; Yu, H.; Xu, X.; Han, F.; Lubineau, G. Ultrasensitive, stretchable strain sensors based on fragmented carbon nanotube papers. *Appl. Mater. Interfaces* **2017**, *9*, 4835–4842. [[CrossRef](#)] [[PubMed](#)]
19. Sun, H.; Lu, Y.; Chen, Y.; Yue, Y.; Jiang, S.; Xu, X.; Mei, C.; Xiao, H.; Han, J. Flexible environment-tolerant electroluminescent devices based on nanocellulose-mediated transparent electrodes. *Carbohydr. Polym.* **2022**, *296*, 119891. [[CrossRef](#)] [[PubMed](#)]
20. Niu, Z.; Cheng, W.; Cao, M.; Wang, D.; Wang, Q.; Han, J.; Long, Y.; Han, G. Recent advances in cellulose-based flexible triboelectric nanogenerators. *Nano Energy* **2021**, *87*, 106175. [[CrossRef](#)]
21. Wang, J.; Euring, M.; Ostendorf, K.; Zhang, K. Biobased materials for food packaging. *J. Bioresour. Bioprod.* **2022**, *7*, 1–13. [[CrossRef](#)]
22. Zhang, Y.; Liu, X.; Li, Y.; Chen, Y. Stabilization of oil-in-water emulsions by nanocellulose: A review. *J. Colloid Interface Sci.* **2018**, *518*, 12–22.
23. Le, H.D.; Loveday, S.M.; Singh, H.; Sarkar, A. Pickering emulsion stabilized by hydrophobically modified cellulose nanocrystals: Responsiveness to pH and ionic strength. *Food Hydrocoll.* **2020**, *99*, 105344.
24. Dong, H.; Ding, Q.; Jiang, Y.; Han, W. Pickering emulsions stabilized by spherical cellulose nanocrystals. *Carbohydr. Polym.* **2021**, *265*, 118101. [[CrossRef](#)] [[PubMed](#)]
25. Varanasi, S.; Henzel, L.; Mendoza, L.; Prathapan, R.; Batchelor, W.; Tabor, R.; Garnier, G. Pickering emulsion electrostatically stabilized by cellulose nanocrystals. *Front. Chem.* **2018**, *6*, 409. [[CrossRef](#)]

26. Ma, T.; Cui, R.; Lu, S.; Hu, X.; Xu, B.; Song, Y.; Hu, X. High internal phase Pickering emulsion stabilized by cellulose nanocrystals for 3D printing. *Food Hydrocoll.* **2022**, *125*, 107418. [[CrossRef](#)]
27. Saidane, D.; Perrin, E.; Cherhal, F.; Guellec, F.; Capron, I. Some modification of cellulose nanocrystals for functional Pickering emulsions. *Philos. Trans. R. Soc. A* **2016**, *374*, 20150139. [[CrossRef](#)]
28. Wu, B.; Yang, C.; Xin, Q.; Kong, L.; Eggersdorfer, M.; Ruan, J.; Zhao, P.; Shan, J.; Liu, K.; Chen, D.; et al. Attractive Pickering emulsion gels. *Adv. Mater.* **2021**, *33*, 2102362. [[CrossRef](#)] [[PubMed](#)]
29. Sun, Z.; Yang, C.; Wang, F.; Wu, B.; Shao, B.; Li, Z.; Chen, D.; Yang, Z.; Liu, K. Biocompatible and pH-responsive colloidal surfactants with tunable shape for controlled interfacial curvature. *Angew. Chem.* **2020**, *59*, 9365–9369. [[CrossRef](#)] [[PubMed](#)]
30. Sun, Z.; Yan, X.; Xiao, Y.; Hu, L.; Eggersdorfer, M.; Chen, D.; Yang, Z.; Weitz, D.A. Pickering emulsions stabilized by colloidal surfactants: Role of solid particles. *Particuology* **2022**, *64*, 153–163. [[CrossRef](#)]
31. Ataiean, P.; Shi, Q.; Ioannidis, M.; Tam, K.C. Effect of hydrophobic modification of cellulose nanocrystal (CNC) and salt addition on Pickering emulsions undergoing phase-transition. *Carbohydr. Polym. Technol. Appl.* **2022**, *3*, 100201.
32. Ni, Y.; Fan, L.; Sun, Y. Interfacial properties of cellulose nanoparticles with different lengths from ginkgo seed shells. *Food Hydrocoll.* **2020**, *109*, 106121. [[CrossRef](#)]
33. Saffarionpour, S. Nanocellulose for stabilization of Pickering emulsions and delivery of nutraceuticals and its interfacial adsorption mechanism. *Food Bioprocess Technol.* **2020**, *13*, 1292–1328. [[CrossRef](#)]
34. Capron, I.; Rojas, O.J.; Bordes, R. Behavior of nanocellulose at interfaces. *Curr. Opin. Colloid Interface Sci.* **2017**, *29*, 83–95. [[CrossRef](#)]
35. Gong, X.; Wang, Y.; Chen, L. Enhanced emulsifying properties of wood-based nanocrystals as Pickering emulsion stabilizer. *Carbohydr. Polym.* **2017**, *169*, 295–303. [[CrossRef](#)] [[PubMed](#)]
36. Kalashnikova, I.; Bizot, H.; Cathal, B.; Capron, I. New Pickering emulsions stabilized by bacterial cellulose nanocrystals. *Langmuir* **2011**, *27*, 7421–7479. [[CrossRef](#)]
37. Aw, Y.Z.; Lim, H.P.; Low, L.E.; Singh, S.K.S.; Chan, E.S.; Tey, B.T. Cellulose nanocrystal (CNC)-stabilized Pickering emulsion for improved curcumin storage stability. *LWT* **2022**, *159*, 113249. [[CrossRef](#)]
38. Pal, R. *Rheology of Particulate Dispersions and Composites*; CRC Press: Boca Raton, FL, USA, 2007.
39. Pal, R. Rheology of polymer-thickened emulsions. *J. Rheol.* **1992**, *36*, 1245–1259. [[CrossRef](#)]
40. Pal, R. Effect of droplet size on the rheology of emulsions. *AIChE J.* **1996**, *42*, 3181–3190. [[CrossRef](#)]
41. Pal, R. Rheology of high internal phase ratio emulsions. *Food Hydrocoll.* **2006**, *20*, 997–1005. [[CrossRef](#)]
42. Zhu, Y.; Gao, H.; Liu, W.; Zou, L.; McClements, D.J. A review of the rheological properties of dilute and concentrated food emulsions. *J. Texture Stud.* **2020**, *51*, 45–55. [[CrossRef](#)]
43. Morfo, Z.; Murray, B.S.; Sarkar, A. Water-in-oil emulsions stabilized by surfactants, biopolymers and/or particles: A review. *Trends Food Sci. Technol.* **2020**, *104*, 49–59.
44. Sarkar, A.; Dickinson, E. Sustainable food-grade Pickering emulsions stabilized by plant-based particles. *Curr. Opin. Colloid Interface Sci.* **2020**, *49*, 69–81. [[CrossRef](#)]
45. Yang, Y.; Fang, Z.; Chen, X.; Zhang, W.; Xie, Y.; Chen, Y.; Liu, Z.; Yuan, W. An overview of Pickering emulsions: Solid-particle materials, classification, morphology, and applications. *Front. Pharmacol.* **2017**, *8*, 287. [[CrossRef](#)]
46. Angkuratipakorn, T.; Sriprai, A.; Tantrawong, S.; Chaiyasit, W.; Singkhonrat, J. Fabrication and characterization of rice bran oil-in-water Pickering emulsion stabilized by cellulose nanocrystals. *Colloids Surf. A Physicochem. Eng. Asp.* **2017**, *522*, 310–319. [[CrossRef](#)]
47. Pal, R. A simple model for the viscosity of Pickering emulsions. *Fluids* **2017**, *3*, 2. [[CrossRef](#)]
48. Binks, B.P.; Clint, J.H.; Whitby, C.P. Rheological behavior of water-in-oil emulsions stabilized by hydrophobic bentonite particles. *Langmuir* **2005**, *21*, 5307–5316. [[CrossRef](#)]
49. Wolf, B.; Lam, S.; Kirkland, M.; Frith, W.J. Shear-thickening of an emulsion stabilized with hydrophilic silica particles. *J. Rheol.* **2007**, *51*, 465–478. [[CrossRef](#)]
50. Katepalli, H.; John, V.T.; Tripathi, A.; Bose, A. Microstructure and rheology of particle stabilized emulsions: Effects of particle shape and inter-particle interactions. *J. Colloid Interface Sci.* **2017**, *485*, 11–17. [[CrossRef](#)]
51. Braisch, B.; Kohler, K.; Schuchmann, H.P.; Wolf, B. Preparation and flow behavior of oil-in-water emulsions stabilized by hydrophilic silica particles. *Chem. Eng. Technol.* **2009**, *32*, 1107–1112. [[CrossRef](#)]
52. Ganley, W.J.; Van Duijneveldt, J.S. Controlling the rheology of montmorillonite stabilized oil-in-water emulsions. *Langmuir* **2017**, *33*, 1679–1686. [[CrossRef](#)] [[PubMed](#)]
53. Hermes, M.; Clegg, P.S. Yielding and flow of concentrated Pickering emulsions. *Soft Matter* **2013**, *9*, 7568–7575. [[CrossRef](#)]
54. Lee, E.; Kim, D.; Kim, K. Distinctive rheological properties of Pickering emulsions: From their origin to the applications. *Korea-Aust. Rheol. J.* **2022**, *34*, 91–103. [[CrossRef](#)]
55. Miao, C.; Mirvakili, M.; Hamad, W.Y. A rheological investigation of oil-in-water Pickering emulsions stabilized by cellulose nanocrystals. *J. Colloid Interface Sci.* **2022**, *608*, 2820–2829. [[CrossRef](#)] [[PubMed](#)]
56. Pandey, A.; Derakhshandeh, M.; Kedzior, S.A.; Pilapil, B.; Shomrat, N.; Segal-Peretz, T.; Bryant, S.L.; Trifkovic, M. Role of interparticle interactions on microstructural and rheological properties of cellulose nanocrystal stabilized emulsions. *J. Colloid Interface Sci.* **2018**, *532*, 808–818. [[CrossRef](#)]

57. Bai, L.; Lv, S.; Xiang, W.; Huan, S.; McClements, D.J. Oil-in-water Pickering emulsions via microfluidization with cellulose nanocrystals: 1. Formation and stability. *Food Hydrocoll.* **2019**, *96*, 699–708. [[CrossRef](#)]
58. Velandia, S.F.; Marchal, P.; Lemaitre, C.; Sadtler, V.; Roques-Carmes, T. Evaluation of the repartition of the particles in Pickering emulsions in relation with their rheological properties. *J. Colloid Interface Sci.* **2021**, *589*, 286–297. [[CrossRef](#)]
59. Shafiei-Sabet, S.; Hamad, W.Y.; Hatzikiriakos, S.G. Rheology of nanocrystalline cellulose aqueous suspensions. *Langmuir* **2012**, *28*, 17124–17133. [[CrossRef](#)]
60. Kadar, R.; Fazilati, M.; Nypelo, T. Unexpected microphase transitions in flow towards nematic order of cellulose nanocrystals. *Cellulose* **2020**, *27*, 2003–2014. [[CrossRef](#)]
61. Pignon, F.; Challamel, M.; De Geyer, A.; Elchamaa, M.; Semeraro, E.F.; Hengl, N.; Jean, B.; Putaux, J.; Gicquel, E.; Bras, J.; et al. Breakdown and buildup mechanisms of cellulose nanocrystal suspensions under shear and upon relaxation probed by SAXS and SALS. *Carbohydr. Polym.* **2021**, *260*, 117751. [[CrossRef](#)]
62. Wu, Q.; Meng, Y.; Wang, S.; Li, Y.; Fu, S.; Ma, L.; Harper, D. Rheological behavior of cellulose nanocrystal suspension: Influence of concentration and aspect ratio. *J. Appl. Polym. Sci.* **2014**, *131*, 40525. [[CrossRef](#)]

**Disclaimer/Publisher's Note:** The statements, opinions and data contained in all publications are solely those of the individual author(s) and contributor(s) and not of MDPI and/or the editor(s). MDPI and/or the editor(s) disclaim responsibility for any injury to people or property resulting from any ideas, methods, instructions or products referred to in the content.